A134783

(1)

AD

AMMRC TR 83-44

CERAMIC LIFE PREDICTION METHODOLOGY - HOT SPIN DISC LIFE PROGRAM

August 1983

R. R. BAKER, L. R. SWANK and J. C. CAVERLY
Ford Motor Company
P.O. Box 2053
Dearborn, Michigan 48121

INTERIM REPORT

Contract No. DAAG46-77-C-0028

Prepared for

ARMY MATERIALS AND MECHANICS RESEARCH CENTER
Watertown, Massachusetts 02172

The findings in this report are not to be construed as an official Department of the Army position, unless so designated by other authorized documents.

Mention of any trade names or manufacturers in this report shall not be construed as advertising nor as an official indorsement or approval of such products or companies by the United States Government.

DISPOSITION INSTRUCTIONS

Destroy this report when it is no longer needed.
Do not return it to the originator.

UNCLASSIFIED

SECURITY CLASSIFICATION OF THIS PAGE (When Data Entered)

REPORT DOCUMENTATION PAGE	READ INSTRUCTIONS BEFORE COMPLETING FORM
1. REPORT NUMBER AMMRC TR 83-44	2. GOVT ACCESSION NO. A134783
	3. RECIPIENT'S CATALOG NUMBER
4. TITLE (and Subtitle) CERAMIC LIFE PREDICTION METHODOLOGY - HOT SPIN DISC LIFE PROGRAM	5. TYPE OF REPORT & PERIOD COVERED Interim Report 1 Oct 79 to 30 Sep 82
	6. PERFORMING ORG. REPORT NUMBER
7. AUTHOR(s) R. R. Baker, L. R. Swank and J. C. Caverly	8. CONTRACT OR GRANT NUMBER(s) DAAG46-77-C-0028
9. PERFORMING ORGANIZATION NAME AND ADDRESS Ford Motor Company Room E3172, SRL, P.O. Box 2053 Dearborn, Michigan 48121	10. PROGRAM ELEMENT, PROJECT, TASK AREA & WORK UNIT NUMBERS AMCMS Code: 69200R.88901
11. CONTROLLING OFFICE NAME AND ADDRESS Army Materials and Mechanics Research Center ATTN: DRXMR-K Watertown, Massachusetts 02172	12. REPORT DATE August 1983
	13. NUMBER OF PAGES 39
14. MONITORING AGENCY NAME & ADDRESS(if different from Controlling Office)	15. SECURITY CLASS. (of this report) Unclassified
	15a. DECLASSIFICATION/DOWNGRADING SCHEDULE

16. DISTRIBUTION STATEMENT (of this Report)

Approved for public release; distribution unlimited.

17. DISTRIBUTION STATEMENT (of the abstract entered in Block 20, if different from Report)

18. SUPPLEMENTARY NOTES

19. KEY WORDS (Continue on reverse side if necessary and identify by block number)

Ceramic materials	Test and evaluation	Silicon carbides
Life expectancy	Predictions	Silicon nitrides
Disks	Brittleness	High temperature

20. ABSTRACT (Continue on reverse side if necessary and identify by block number)

DD FORM 1 JAN 73 1473 EDITION OF 1 NOV 65 IS OBSOLETE

UNCLASSIFIED

SECURITY CLASSIFICATION OF THIS PAGE (When Data Entered)

Block No. 20

ABSTRACT

A rotating disc was designed to fail due to time dependent mechanisms. Several discs were fabricated and an existing test rig was developed to test the discs at design conditions. Ten discs were tested at steady state under the design conditions of 2300°F rim temperature and 50,000 rpm for periods of 0.20 hours to 25 hours. An experimental failure distribution was obtained for the ten discs and presented as reliability versus time. Three different data bases (double torsion, stress rate, and stress rupture) were used to calculate reliability versus time and the results were compared to the experimental results. It was observed that the best correlation with the experimental results was given by the stress rupture data base.

FOREWARD

This report presents the work completed during the period of October 1, 1979, through September 30, 1982, on the Hot Spin Disc Life Program, which is part of the "Methodology for Ceramic Life Prediction Program," initiated by Mr. Robert Schulz of the Office of Conservation, Division of Transportation Systems, Department of Energy, and monitored by the Army Materials and Mechanics Research Center under Contract Number DAAG-46-77-C-0028. Funds for this phase of the work were provided by AMMRC. This work was necessary in formulating a methodology for ceramic life prediction so that ceramic materials can be used in high temperature structural applications. The principal investigator of this program was R. R. Baker, Ceramic Materials Department, Engineering and Research Staff, Ford Motor Company. The technical monitor was Dr. E. M. Lenoe of AMMRC. The authors wish to thank Drs. E. M. Lenoe, R. N. Katz, and Mr. G. D. Quinn of AMMRC for suggestions in carrying out the program, and Mr. A. F. McLean, Manager, Ceramic Materials Department, Ford Motor Company, for careful reading and constructive criticism of the report.

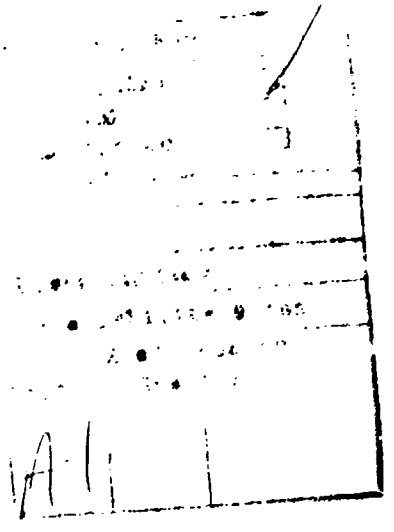

TABLE OF CONTENTS

INTRODUCTION

Since the early sixties there has been considerable interest in silicon nitride as an engineering material. Sage and Histed[1] reviewed some of the applications for silicon nitride and suggested the use of silicon nitride in gas turbines. A potential increase of 100°C in turbine stator blade service temperature was forecast. Glenny and Taylor[2] reviewed the material properties of silicon nitrides and noted the high strength at elevated temperatures of silicon nitride. Evans and Wiederhorn[3] observed the phenomenon of static fatigue in hot pressed silicon nitride, and noted that this presented a design problem in the application of the material in highly stressed applications at elevated temperatures.

The phenomenon of static fatigue is well known in metals where it may be caused by slow crack growth. Siverns and Price[4] observed that the crack growth rate in steel at elevated temperatures was correlated with the slow crack growth power equation

$$V = AK_I^n \qquad (1)$$

Evans and Johnson[5] suggested that this equation could be applied to ceramics and that the cause of slow crack growth was grain boundary sliding. This is due to the glassy phases in the grain boundary softening at elevated temperature and allowing the crystalline grains of silicon nitride to slide relative to one another at the tip of the crack where the stresses are the highest. The sliding of the grains causes the crack to grow and continued application of stress and temperature could cause catastrophic failure[6].

Williams and Evans[7] proposed the double torsion test to measure the values of the crack velocity exponent, and the premultiplier in Eqn. 1. The double torsion test is a simple test in concept, that loads a pre-cracked specimen in a manner that the stress intensity factor remains constant as the crack grows. This simplifies the analysis and makes it possible to determine A and n from the load versus time curve.

Charles[8] proposed stress rate testing to determine the crack velocity exponent and demonstrated its use on glass. In stress rate testing MOR bars are fractured at two different stress rates to obtain two pairs of data - the fast fracture stress and its corresponding stress rate. From these sets of data the slow crack growth parameters are calculated.

Several experimenters have conducted stress rupture tests on ceramic materials. Trantina[9] conducted stress rupture tests on Norton's NC-132 material, a hot pressed silicon nitride. His tests were conducted in three-point bending on bars of 0.9 inch span with a cross section of 0.1 inch x 0.1 inch. Quinn[10] conducted stress rupture tests on several different structural ceramic materials. His tests were conducted in four-point bending on a fixture with a 1.5 inch outer span, a 0.75 inch inner span, and a bar with a 0.110 inch base and a 0.085 inch height.

Previous experimenters conducted their tests on small parts with very small volumes compared to the volume of typical gas turbine components. Previous tests were also conducted at uniform temperatures, but gas turbine components have large temperature gradients. This suggested the need for generating a time to failure data base on a component the size of a typical gas turbine component with temperature and stress distributions similar to gas turbine components. This data base could then be used as a test case for evaluation of models of failure and computer programs used to predict time to failure.

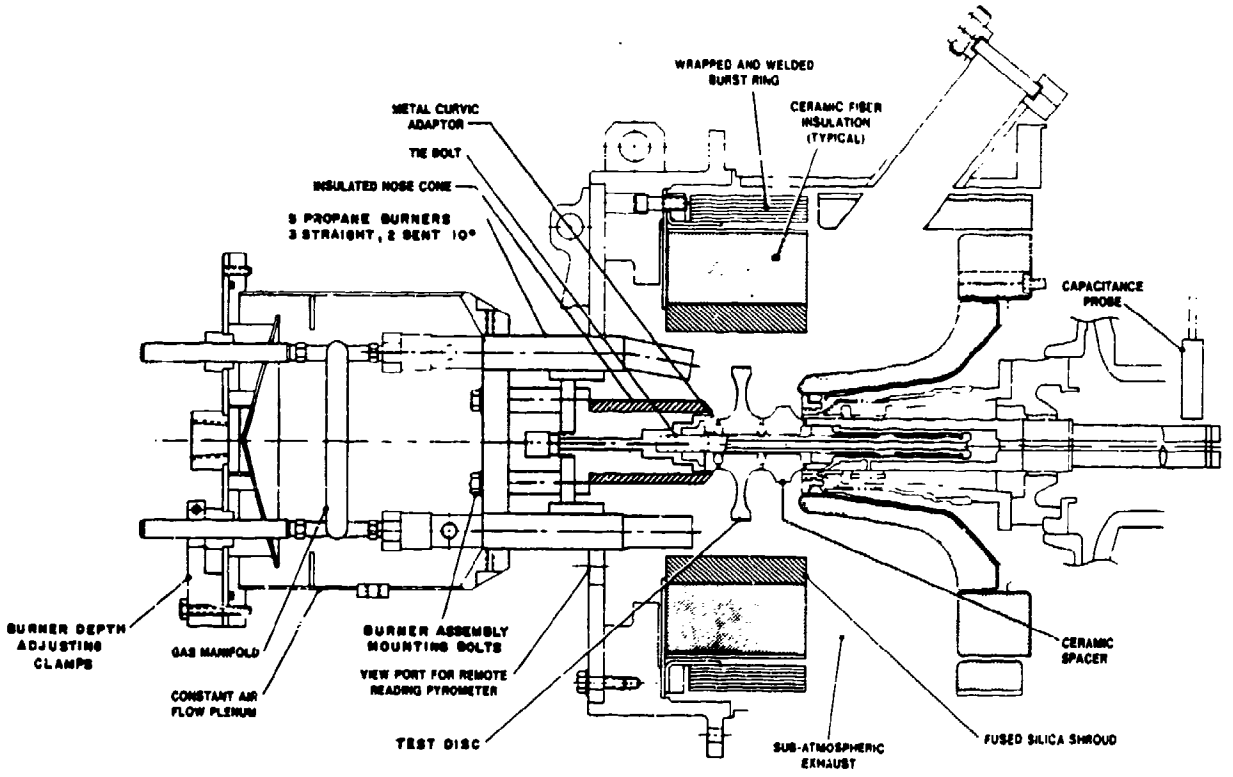

Figure 1 - Hot-spin test rig

The hot spin rig shown in Fig. 1 was selected for testing of a gas turbine component because it had accumulated many hours of testing and had shown that it could test turbine discs at speeds and temperatures simulating actual engine conditions[11]. The rig development required to meet the test conditions and the initial calibration test were previously described[12]. This report reviews the most recent results with emphasis on the determination of experimental reliability versus time and the comparison to calculated reliability versus time.

II. DESIGN OF THE DISC

A finite element model of the rotating components was set up for calculating the temperatures of the disc. The model is shown in Fig. 2. The physical parts represented by the finite elements are shaded and labeled for identification. The finite elements that compose the model are rectangular or triangular in shape. The material thermal properties used in the analysis are given in Table I.

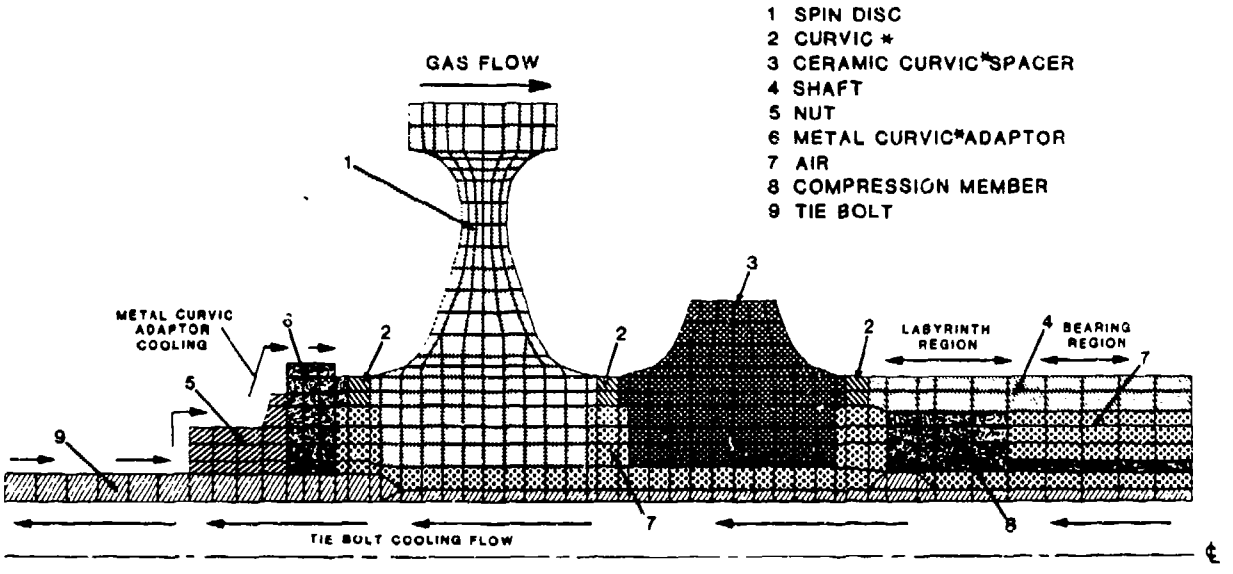

Figure 2 - Rotating components heat transfer model

The temperatures within the rotating components were determined by the boundary conditions and the thermal conductivities of parts in the assembly. Heat was applied to the front face and rim of the spin disc with propane gas burners. The temperature of the front face was measured with a radiation pyrometer and the measured temperatures were used as input to the analysis. The tie bolt was cooled with air as shown on Fig. 2. The cooling air mass flow rate and associated heat transfer coefficients formed the boundry conditions. A portion of the tie bolt cooling air was directed to the metal curvic adaptor for cooling and the mass flow rate and heat transfer coefficients formed the boundary conditions for the exterior of the tie bolt, nut, and metal curvic adaptor. The downstream side of the spin disc and the exterior of the ceramic curvic spacer were heated with hot gases and air swirling in the rig, thus forming another boundary condition. The labyrinth and bearing region on the shaft form the last boundary condition. As part of the model, radiation heat transfer was included between the spin disc bore, ceramic curvic spacer bore and the tie bolt.

*TM

Calculated temperature distributions were compared to results from temperature sensitive paints and adjustments to the model were made to obtain agreement. Temperature measurements of the air in the cooling streams were also used as input to the model and as a check on the validity of the model; for example the temperature of the tie bolt cooling air was measured as it entered the labyrinth and as it left the tie bolt. The temperature of the air in the labyrinth region was used as input to the model and the air exit temperature was compared to the calculated value as a check on the model.

Figure 3 illustrates the finite element grid used to calculate the stresses in the spin disc. The temperature distribution was derived from the heat transfer model and transferred to the stress finite element grid. The temperature contour plot at the test design conditions is illustrated in Fig. 4. The combined thermal and centrifugal stresses, at the test condition, are illustrated in Figs. 5 through 9. These stress plots show the maximum principal tensile stress, the tangential stress, the radial stress, the axial stress, and the maximum shear stress.

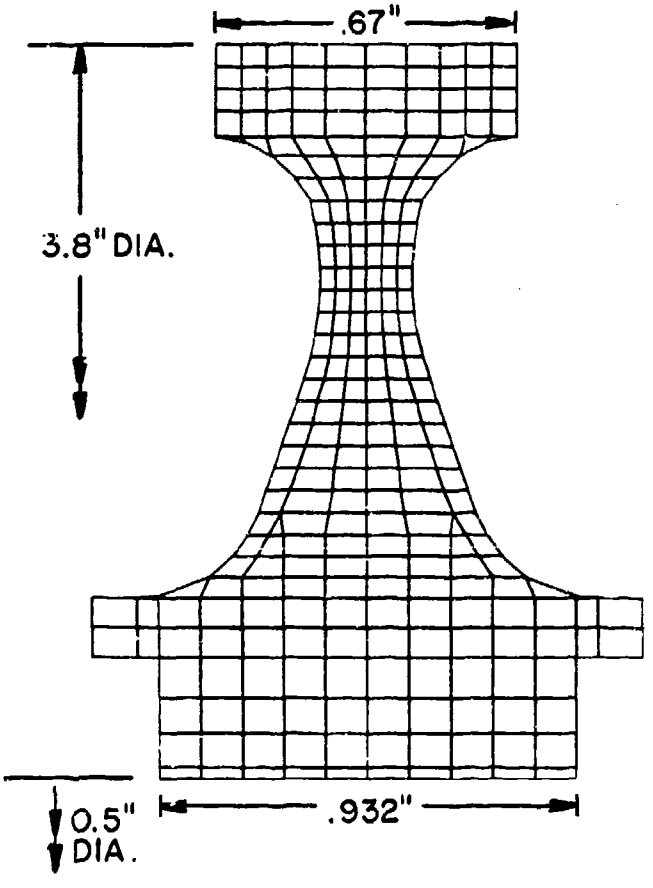

Figure 3 - Disc finite element grid

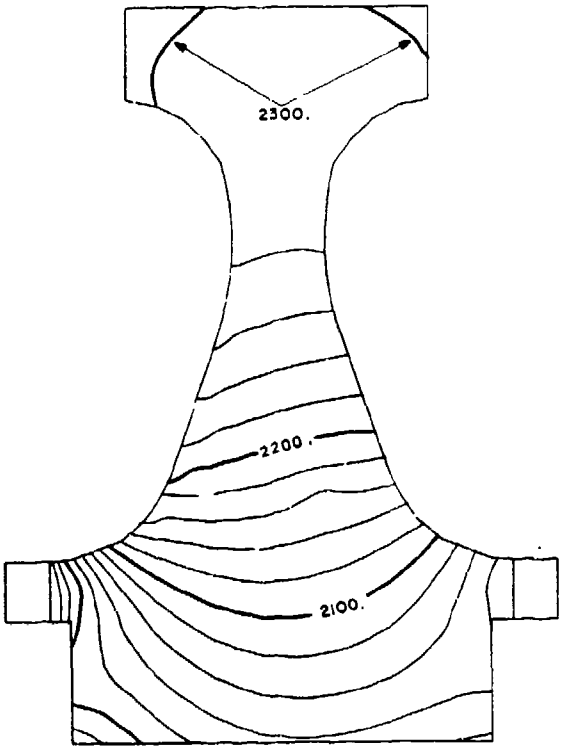

Figure 4 - Isotherms [°F] in disc at 50,000 rpm.

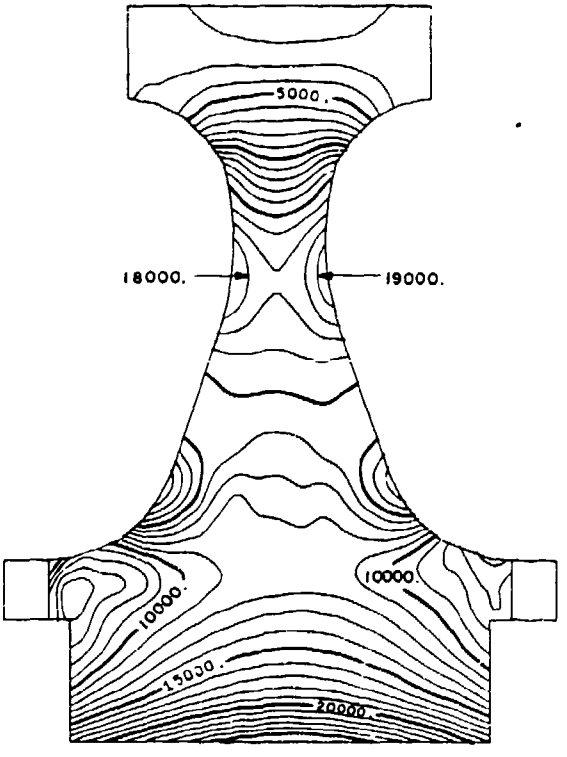

Figure 5 - Maximum principal stresses [psi] in disc combining thermal and centrifugal stresses at 50,000 rpm.

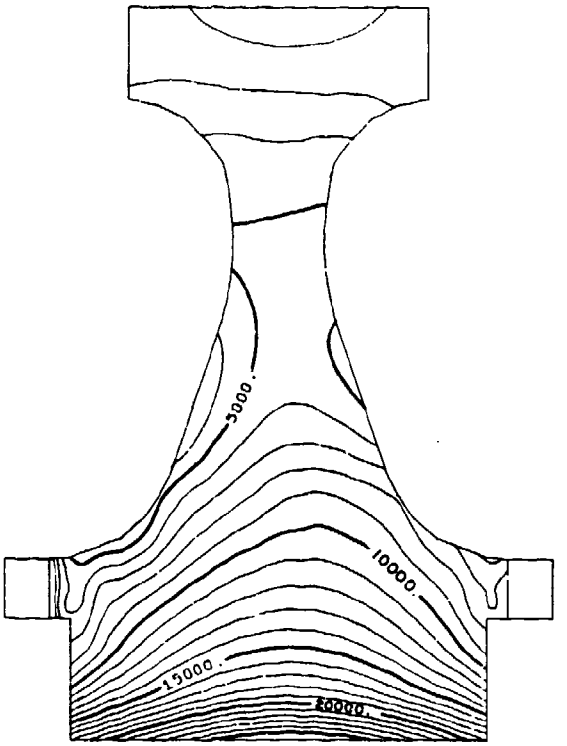

Figure 6 - Tangential stresses [psi] in disc combining thermal and centrifugal stresses at 50,000 rpm.

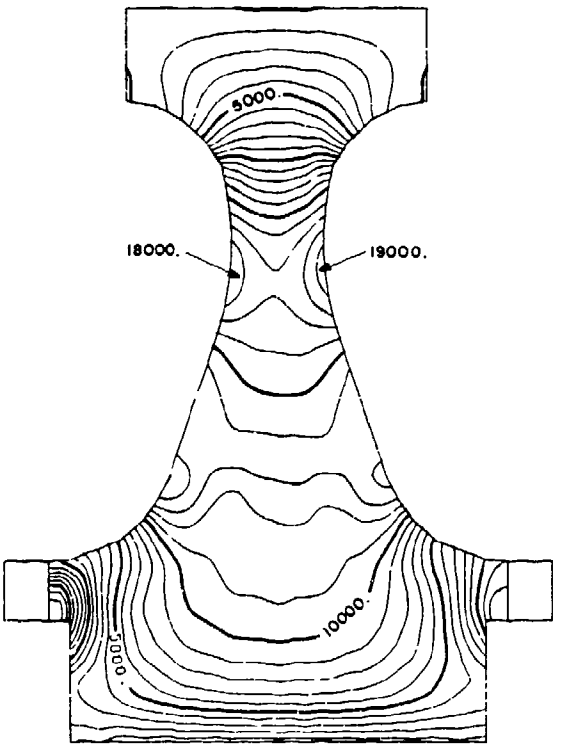

Figure 7 - Radial stresses [psi] in disc combining thermal and centrifugal stresses at 50,000 rpm.

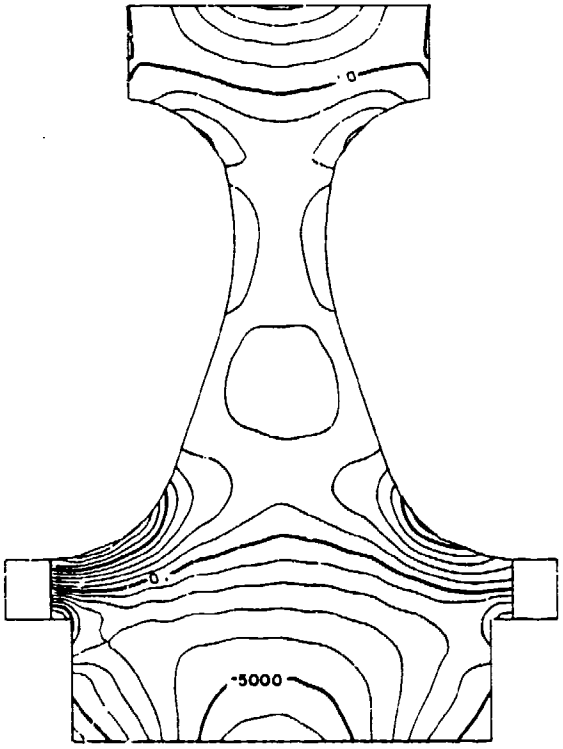

Figure 8 - Axial stresses [psi] in disc combining thermal and centrifugal stresses at 50,000 rpm.

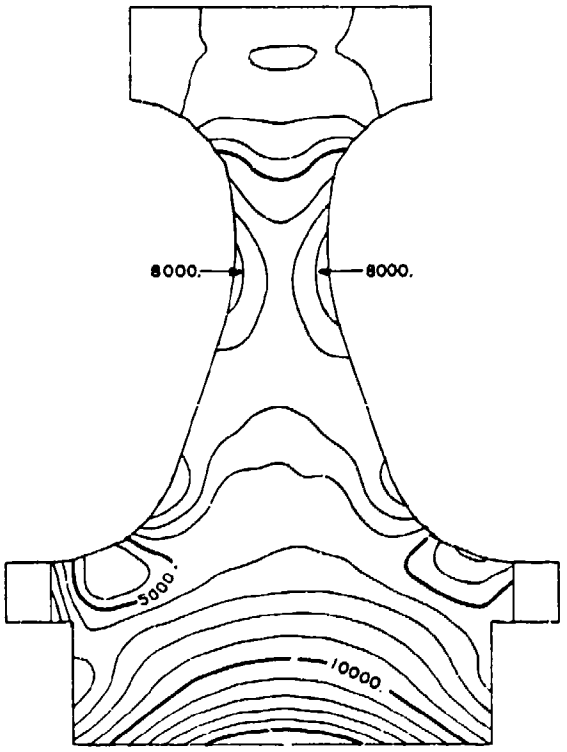

Figure 9 - Maximum shear stresses [psi] in disc combining thermal and centrifugal stresses at 50,000 rpm.

The previous figures illustrate the combined thermal and mechanical stress conditions at which the stress rupture tests were conducted. The mechanical stresses due to centrifugal loads at 50,000 rpm were calculated with the disk at a constant temperature of 78°F, and the stresses are plotted in Figs. 10 through 14. These stress plots show the maximum principal tensile stress, the tangential stress, the radial stress, the axial stress, and the maximum shear stress, and may be compared to the combined stresses of Figs. 5 through 9. The elastic properties used in the stress calculations are given in Table II.[13]

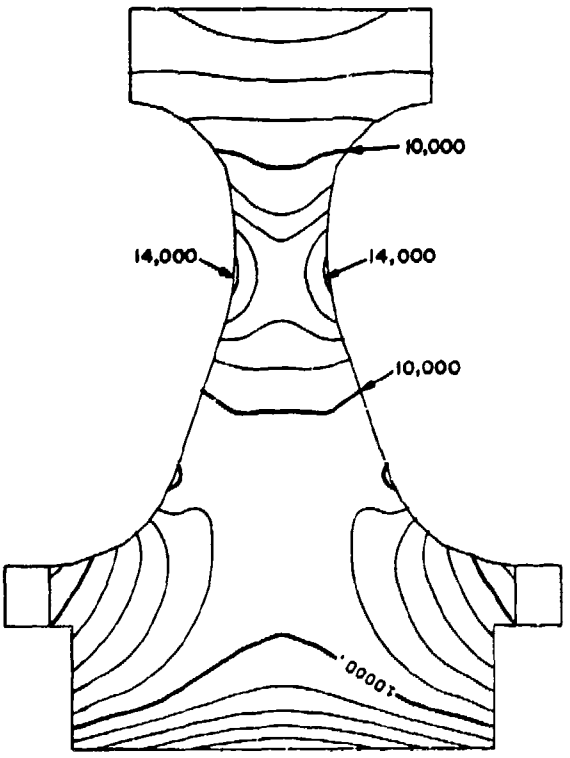

Figure 10 - Maximum principal stresses [psi] in disc, centrifugal stresses at 50,0000 rpm.

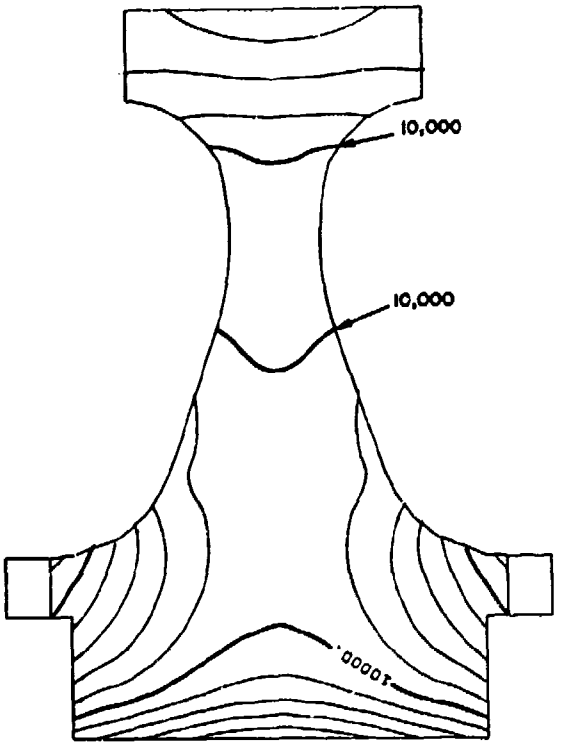

Figure 11 - Tangential stresses [psi] in disc, centrifugal stresses of 50,000 rpm.

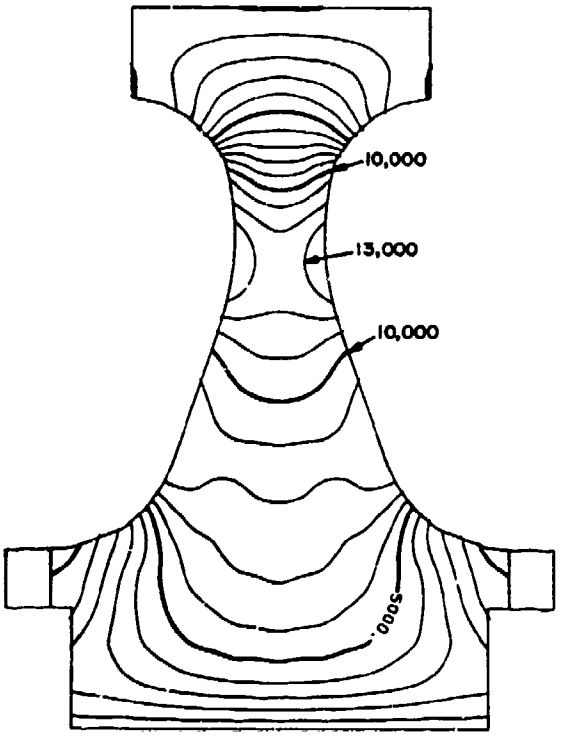

Figure 12 - Radial Stresses [psi] in disc, centrifugal stresses at 50,000 rpm.

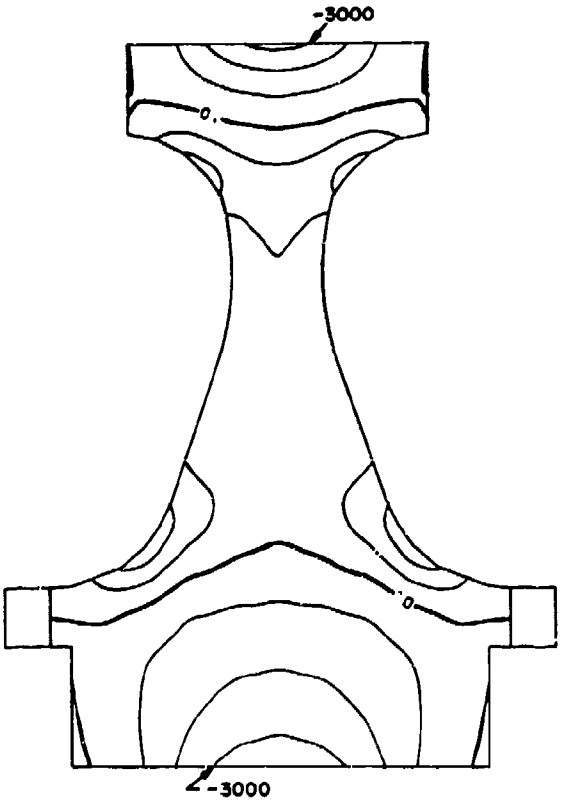

Figure 13 - Axial stresses [psi] in disc, centrifugal stresses at 50,000 rpm.

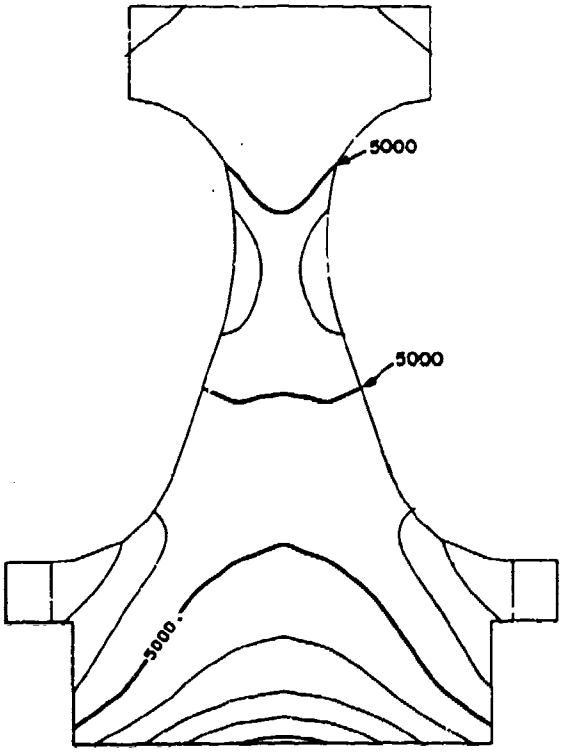

Figure 14 - Maximum shear stresses [psi] in disc, centrifugal stresses at 50,000 rpm.

Three data bases: double torsion, stress rate, and stress rupture, were available for the calculation of time dependent reliabilities. The first two data bases are used with a formula derived by Paluszny[13] and repeated here as Equation 2. Definition of the symbols is given in Appendix C.

$$R = \exp - \left[\left[(\ln \frac{1}{R_{ff}})^{\frac{n-2}{m}} + \frac{\sigma^n t}{\sigma_\theta^{n-2} B}\right]^{\frac{m}{n-2}}\right] \qquad (2)$$

During this work, Eqn. 2 was reduced to a simpler form shown as Eqn. 3. The detailed algebraic steps are given in the interim report[12].

$$R = R_{ff}^{(1+\frac{\sigma^2 t}{B})^{\frac{m}{n-2}}} \qquad (3)$$

Equation 3 is much simpler for computation and was programmed for digital computer use to calculate time-dependent reliabilities for steady state temperature and loading conditions. The equation was evaluated for each element of the finite element grid of Fig. 3 using the maximum principal stress, the Weibull modulus, the crack velocity exponent, the value of B, and the fast fracture reliability of the

element. The Weibull modulus, crack velocity exponent, and the value of B were linearly interpolated from a table of these parameters versus temperatures, based on the centroidal temperature of the element.

Equation 3 shows that when time equals zero the time dependent reliability is simply the fast fracture reliability. The fast fracture reliability was evaluated by integrating the normal stress around the unit sphere in each finite element and evaluating the Weibull volume integral for each element[15,16,17]. The double torsion and stress rate data bases yield the parameters "B" and "n" essential for the evaluation of Eqn. 3. Figure 15 shows the calculation flow path utilizing double torsion data. Fast fracture testing produced a collection of fast fracture data which was analyzed with maximum likelihood estimation methods[18] to determine the characteristic modulus of rupture and the Weibull modulus. The stress and temperature distributions from finite element analysis along with the Weibull parameters were input to a computer program which evaluated Weibull's formula for fast fracture reliability, which in turn was input to another computer program which calculated time dependent reliability. From double torsion testing the crack velocity exponent, the premultiplier "A", and the critical stress intensity factor were obtained. With these parameters and the value of the stress intensity factor coefficient, "Y", the value of "B" was calculated[14]. The value of "B" and crack velocity exponent "n" were input to a computer program that evaluated the reliability versus time.

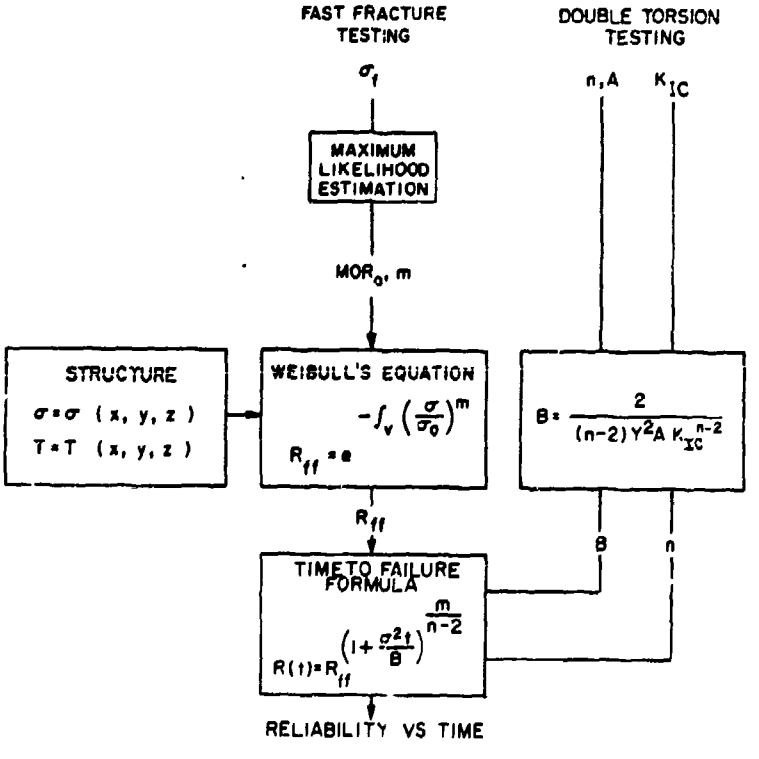

Figure 15 - Calculation flow path utilizing double torsion data

Figure 16 shows the calculation flow path utilizing stress rate testing data to obtain reliability versus time. Stress rate testing determined pairs of fast fracture strength and the corresponding value of stress rate. The value of "B" and the crack velocity exponent "n" were calculated from the pairs of strength and stress rate with the formulas shown[19,20]. The fast fracture calculation was the same as that used with double torsion data.

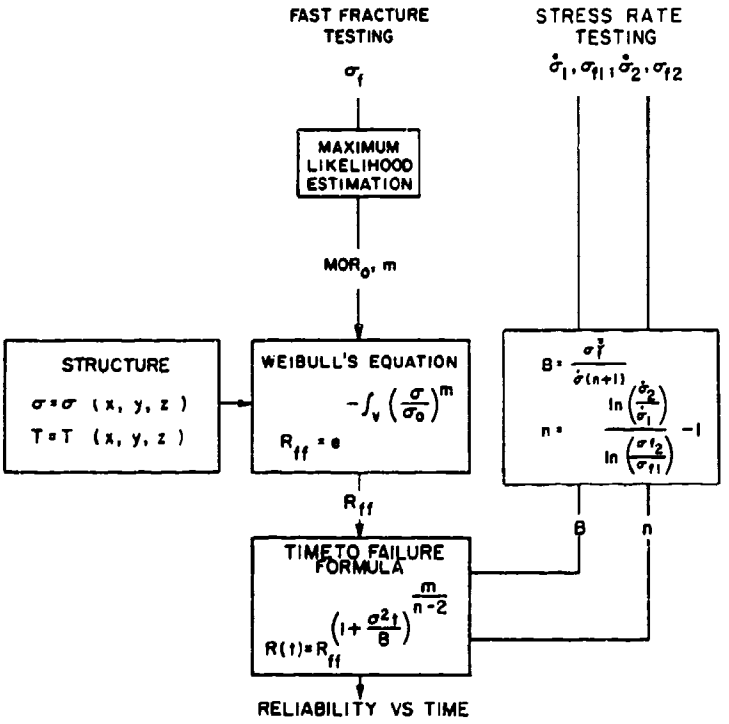

Figure 16 - Calculation flow path utilizing stress rate data

The third data base available for predicting time dependent reliability is stress rupture testing. Quinn[10], Trantina[9], and Govila[21] have done extensive stress rupture testing on NC-132. An empirical formula suitable for the calculation of time dependent reliability using stress rupture data is given in Appendix A. The calculation flow path is shown in Fig. 17. The reliability versus time formula was evaluated for each element in the finite element mesh. The fast fracture reliability calculation is the same as that used for the double torsion and stress rate data bases.

The procedures outlined here were used to design the disc. The design was arrived at by checking trial designs with the reliability versus time calculation procedures until a satisfactory design was obtained. The reliability versus time for the final design and test conditions is shown in Fig. 18. Note the widely different results for the different data bases.

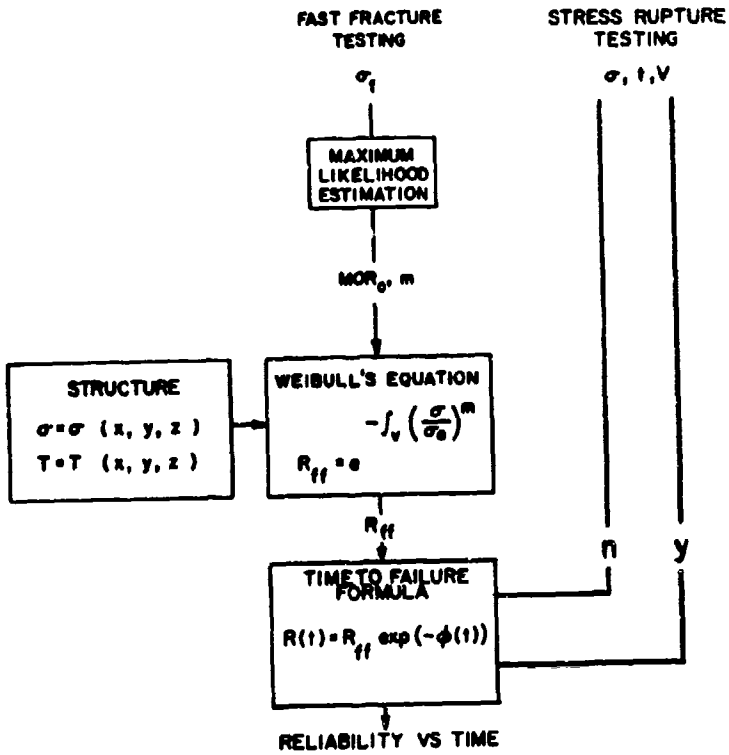

Figure 17 - Calculation flow path utilizing stress rupture data

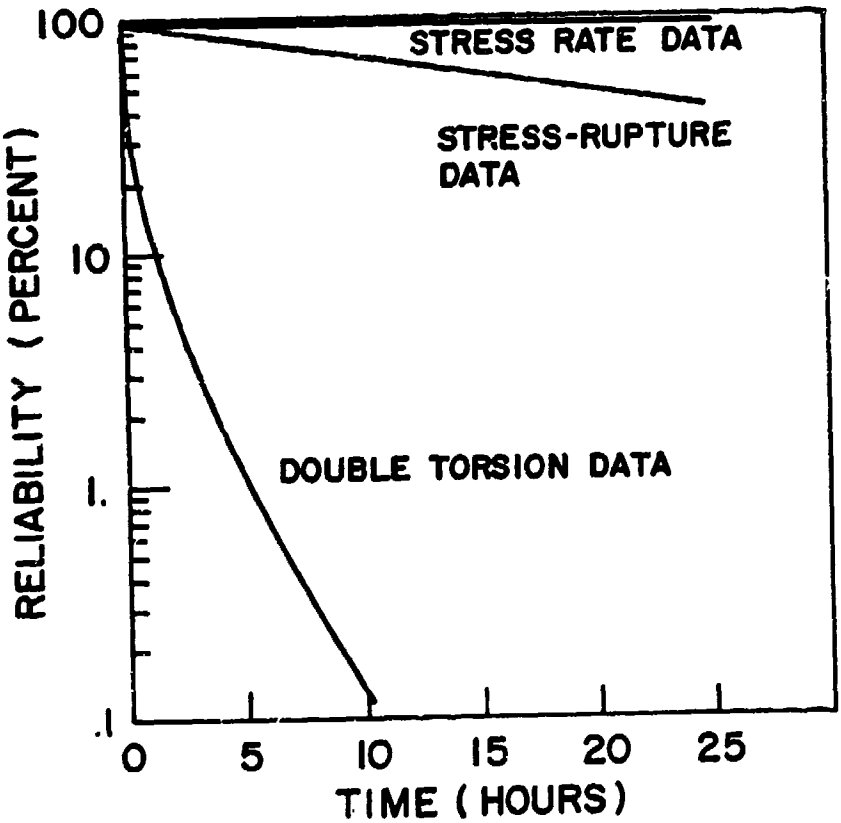

Figure 18 - Calculated reliability versus time.

III. DISC MACHINING

Life prediction discs were machined from six inch square, one and three-eighths inch thick billets of hot pressed silicon nitride (NC132).* The four inch diameter discs were made in several steps beginning with a slicing operation in which an octagonal block was cut out of each billet. This piece was ground to the approximate thickness of the finished disc and a center hole or bore was then core drilled through with a diamond core drill. The bore was then ground to finish size allowing the disc to be centrally mounted for further grinding operations. Most of the grinding was done on a Brown and Sharp Universal grinder. Initial material removal was accomplished using 120-150 grit diamond plate wheel and a commercial water soluble coolant (X50-2 Chem-trend). Final dimensions were produced with 200-250 grit wheels. The disc face contours were produced by specially shaped contour grinding wheels as shown in Fig. 19. These wheels were rotated at 12-1300 rpm and were fed into the disc side in a three step operation as shown in Fig. 20. The disc was rotated at 100 rpm in the opposite direction to the grinding wheel which allowed control of the grinding and stability of the setup. Finish grinding of the disk face removed .0001 inch of material per revolution while advancing radially at a rate of .0003 to .0005 per revolution. Grinding wheel speed was 7000 rpm.

All grinding tools, including contour wheels, were diamond coated and final polishing of the disc contours was done with diamond pastes on a brass lap. The lap was in the form of a ball on a 1/4" diameter shank and the lap was driven by a hand held electric drill. The disc was slowly rotated on an arbor and the contour was polished to a 1-2 μ inch finish by successively using diamond pastes of 30-40, 6-12 and 1-5 micron grit.

Finally the curvic couplings used to mount the disc to the shaft were ground by diamond coated grinding wheels on special purpose curvic grinding equipment. The discs were then Zygloed for possible cracks caused by grinding and then dimensionally inspected. Figure 21 shows the completed disc ready for testing.

---

* Certified Billets from Norton Company

Figure 19 - Contour Grinding Wheel

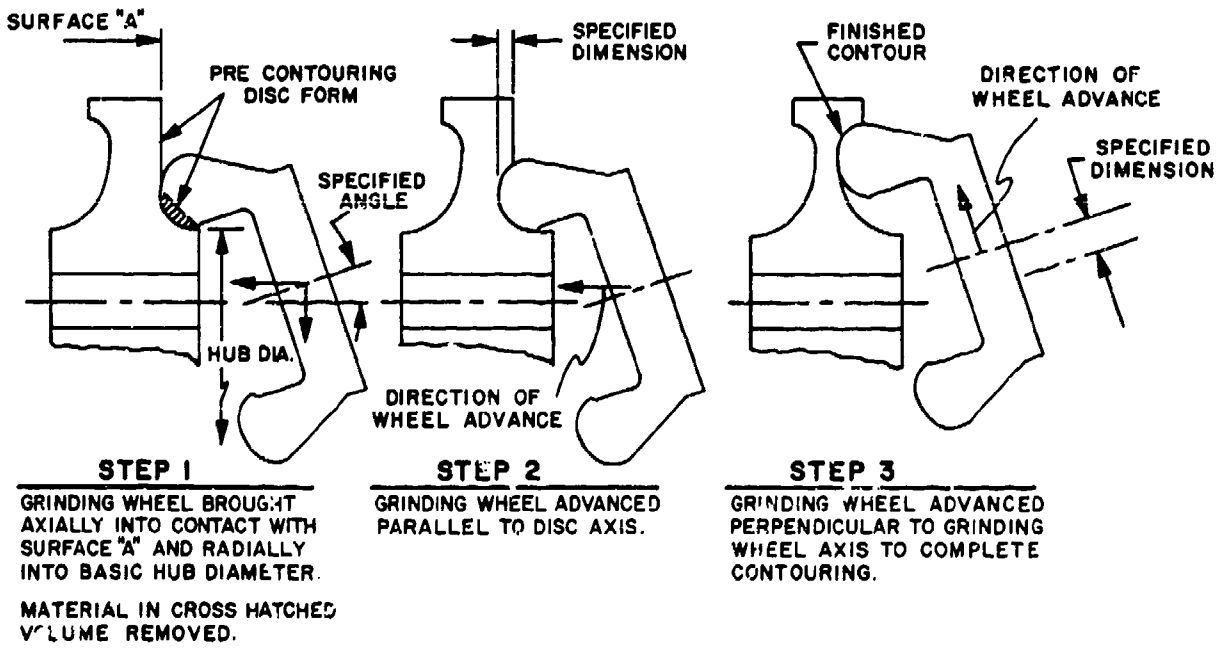

Figure 20 - Procedure for disc contouring

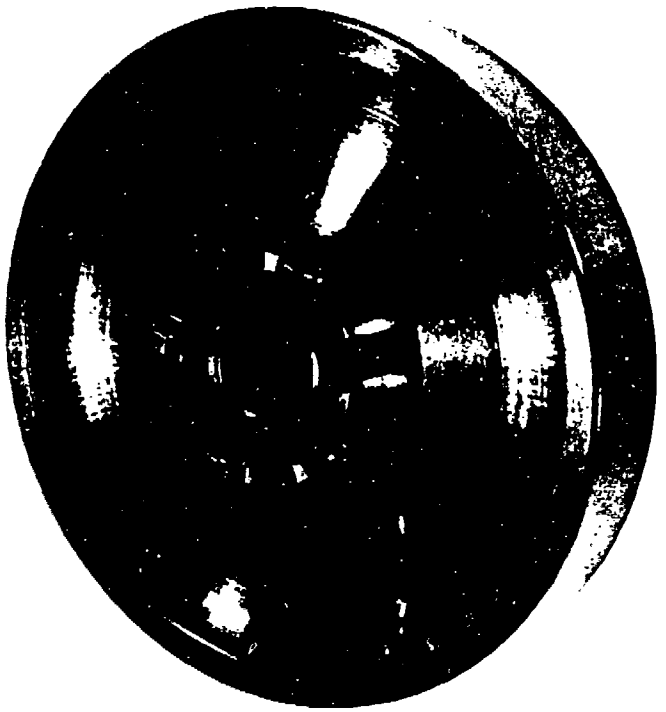

Figure 21 - Disc ready for testing

Figure 22 shows a 10X photograph of the disc throat region ready for testing.

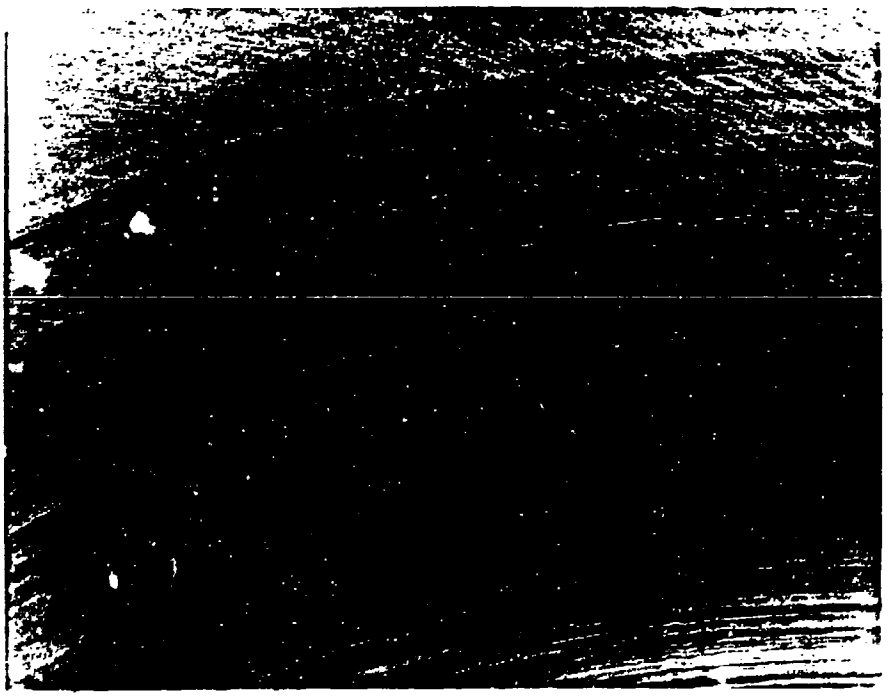

Figure 22 - Disc throat region at 10X

IV. TEST PROGRAM

All the data required to analyze the rig performance and the conditions affecting the rotor were recorded on a magnetic tape recorder. The tape had a four hour running cycle after which it was changed and the tape erased if the running period had been uneventful. If a failure had occurred, the magnetic tape was played back into a Data Trak recorder on to light sensitive recording paper. The resulting traces gave continuous records of rig speed, disk surface temperature, cooling air flows etc. right thru a failure. The channels of the Data Trak were carefully calibrated before testing began and scaled Mylar overlays allowed the running parameters during a failure to be very accurately measured.

These records invariably showed smooth steady state running conditions right to the very instant of disk failure at which time an instantaneous change in disk temperature would occur followed by slight changes in oil pressure, cooling air flows etc.

The disc face temperature, displayed on the tapes, was measured by an Ircon radiation pyrometer which viewed the face of the spinning heated rotor thru a hole in the face plate of the rig. There were no intervening glass windows or other obstructions. This unit had been calibrated using an electric furnace containing a small block of NC 132 thermocoupled with Platium 13% Rhodium couple readout on a Doric meter. The block was heated to a temperature higher than the maximum of the pyrometer range being calibrated, the furnace heating elements were turned off and readings of the thermocouple and radiation pyrometer were taken as the block slowly cooled down thru the range being calibrated. The thermocouple was placed inside the block within 1/8" of the face whose temperature was being measured by the pyrometer. The technique of calibrating during cooling was necessary because the thin, white hot furnace heating elements affected the pyrometer readings. However, when the power was shut off, the heating wires quickly cooled while the block had hardly responded. The thermocouple had a factory accuracy of ± 5°F and this allowed an emissivity setting of .88 to be selected which gave an error of only +10°F at the test temperature of 2300°F. This 10° correction was taken into account when setting the temperature of the disks during actual testing effectively limiting the error of disk temperature measurement to ± 5°F.

Actual testing of a disk was begun with a cold spin test to full test speed (50000 rpm) to assure that no mechanical problem would require a shut down after the disc had been brought to test temperature. The disc was then spun at 2000 rpm and the gas burners were lit and the disc rim allowed to heat up to 1800 - 2000°F range. The speed would then be increased to 10,000 rpm and the rim stabilized at 2100-2200°F. A second speed increase would then take the disc to 24000 rpm and a 15 minute warm up allowed during which bolt cooling air would be carefully adjusted and disc rim would be brought to 2150-2200°F. Holding the rim below 2300°F before reaching 50,000 rpm was necessary because increases in speed had the effect of slightly raising rim temperature all other conditions remaining the same, thus a possible over-tempera e condition was avoided.

When all conditions were throughly stabilized at acceptable levels, the speed was increased to 50,000 rpm and any final rim temperature adjustments necessary to get a 2300°F temperature were made. When the rim came to 2300°F at 50000 rpm the test time was officially begun. This steady state condition was held until the disc either failed or ran for 24 hours. A disk failure was a barely audible "thump" after which the rig ran smoothly along.

Post failure investigations usually showed the disc as well as the spacer and burst ring to be completely shattered. The metal attaching parts, bolt curvic adaptor and nut, were usually found broken off although after several failures the bolt was found in place, straight and neither stretched or over-heated. This was not unexpected since the bolt had originally been designed for a stretch load of 4700 lbs which took it to 80% of its tensile strength at running temperatures. The installation load of only 2500 lbs thus left a very comfortable safety margin and the critical cooling air temperature was measured by a thermocouple at its exit from the bolt making precise control very easy.

V. EXPERIMENTAL RESULTS

A total of twelve discs were tested in the program. The discs were identified by the four digit billet serial number assigned by the Norton Company. Ford Motor added the prefix NC to distinguish these discs from others fabricated by Ford for other programs. Two discs failed on start-up and were not included as part of the database because these failures were probably not due to time dependent phenomena. Disc number NC-1321 was shut-down after thirteen hours of steady state testing, but it failed on an attempted restart so it was considered censored at 13 hours. Disc numbers NC-1319, and NC-1337 were censored at 24 hours and disc NC-1323 was censored at 25 hours. These discs were shut down after continuous steady state testing without failure.

The test results are summarized in Table VI. The survival probability of each disc was calculated with the following formula given by Bury[22].

$$\hat{R}(X') = \prod_{i}^{k} \frac{N-i}{N-i+1} \qquad (4)$$

The format of the table is also taken from Bury. The experimental failures are plotted on Fig. 23 as circles. These points form a data base against which analytical methods of predicting reliability versus time for complex structures can be measured. Also shown on Fig. 23 are the calculated reliabilities versus time from the three data bases used. These are the same as Fig. 18. The results calculated from stress rupture data appear to give the best correlation.

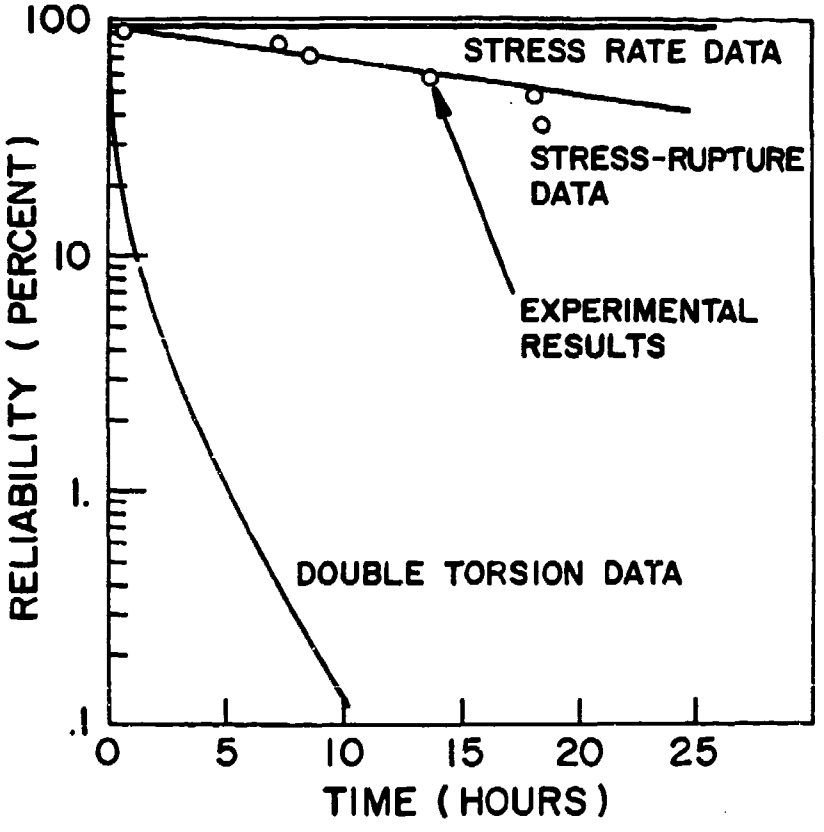

Figure 23 - Experimental and Calculated Reliability Comparison

As an estimate of error in the calculated reliabilities the radiation pyrometer was assumed to have an error of ±20°F and the results were recalculated and plotted on Fig. 24. The stress rate error was too small to appear on the graph but the calculated reliability at 25 hours is 0.966, .961, and .956 for 2280°F, 2300°F and 2320°F maximum material temperatures respectively. The actual pyrometer temperature error was estimated to be ±5°F because it was calibrated with a sample of hot pressed silicon nitride instrumented with a thermocouple. The results in Fig. 24 serve as an upper limit on the experimental and analytical determination of the temperatures and their effect on calculated reliabilities.

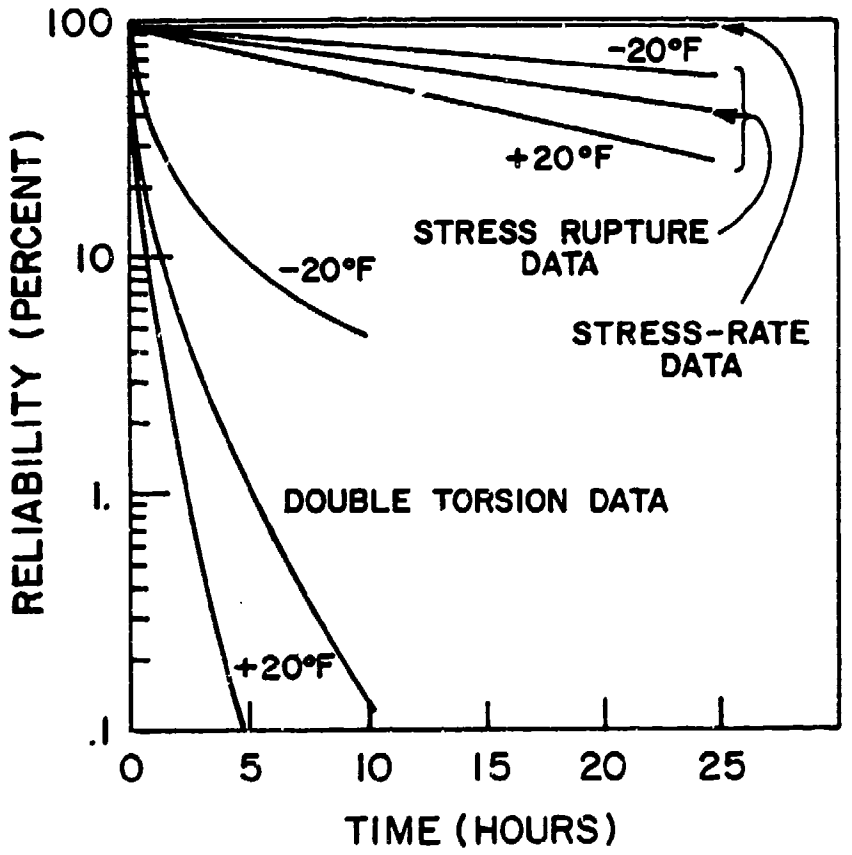

Figure 24 - Effect of estimated errors in temperature upon calculated results.

VI. CONCLUSIONS

The comparison of calculated to experimental results using the three different databases show that stress rupture data is the best for predicting reliability versus time.

VII. RECOMMENDATIONS

Future time dependent reliability investigations should concentrate on stress rupture experimental methods and analytical techniques to predict time dependent reliabilities using stress rupture data.

The discs from the test program were delivered to AMMRC for study, and it is recommended the AMMRC conduct a fractographic investigation of the discs.

REFERENCES

1. Sage, A. M. and Histed, J. H., "Applications of Silicon Nitride," Powder Metallurgy, No. 8, (1961).

2. Glenny, E. and Taylor, T. A., "Mechanical Strength and Thermal Fatigue Characteristics of Silicon Nitride," Powder Metallurgy, No. 8, (1961).

3. Evans, A. G. and Wiederhorn, S. M., "Crack Propagation and Failure Prediction in Silicon Nitride at Elevated Temperatures," Journal of Materials Science, September, 1974.

4. Siverns, M. J., and Price, A. T., "Crack Growth Under Creep Conditions," Nature, November 21, 1970.

5. Evans, A. G., and Johnson, H., "The Fracture Stress and its Dependence on Slow Crack Growth," Journal of Materials Science, No. 10, (1975).

6. Evans, A. G., "High Temperature Slow Crack Growth in Ceramic Materials," Ceramics for High Performance Applications, Ed. John J. Burke, Alvin E. Gorum, and R. Nathan Katz, Chesnut Hill, Massachusetts, Brook Hill, 1974.

7. Williams, D. P., and Evans, A. G., "Simple Method for Studying Slow Crack Growth," Journal of Testing and Evaluation, July, 1973.

8. Charles, R. J., "Dynamic Fatigue of Glass," Journal of Applied Physics, December, 1978.

9. Trantina, G. G., "Strength and Life Prediction for Hot-Pressed Silicon Nitride," Journal of the American Ceramic Society, August, 1979.

10. Quinn, G. D., Characterization of Turbine Ceramics After Long-Term Environmental Exposure, Tech. Rept. AMMRC TR 80-18, April, 1980.

11. DeBell, G. C., and Swank, L. R., Testing of Ceramic Rotors Hot Spin Test Rig and Rotor Preparation, ASME paper 80-GT-144, 1980.

12. Baker, R. R., Swank, L. R., and Caverly, J. C., "Ceramic Life Prediction Methodology - Hot Spin Disc Life Program," Tech. Rept. AMMRC TR 82-26, April, 1982.

13. Uy, J.C., Williams, R. M., and Swank, L. R., Design Properties of Silicon Nitride for High Temperature Gas Turbine Application, ASME paper 77-BT-55, 1977.

14. Paluszny, A. and Nicholls, P. F., "Predicting Time-Dependent Reliability of Ceramic Rotors," Ceramics for High Performan- Application-II. Ed. John J. Burke, Edward N. Lenoe, and R. Nathan Katz, Chesnut Hill, Massachusetts, Brook Hill, 1978.

15. Weibull, W., "A Statistical Theory of the Strength of Materials," Proceedings of the Royal Swedish Institute for Engineering Research, Stockholm, 1939.

16. Vardar, O. and Finnie, I., "An Analysis of the Brazilian Disc Fracture Test Using the Weibull Probabilisitc Treatment of Brittle Strength," International Journal of Fracture, June, 1979.

17. Swank, L. R., and Williams, R. M., "Correlation of Static Strengths and Speeds of Rotational Failure of Structural Ceramics," American Ceramic Society Bulletin, August, 1981.

18. Jeryan, R. A., "Use of Statistics in Ceramic Design and Evaluation," Ceramics for High Performance Applications-II, Ed. John J. Burke, Edward M. Lenoe, and R. Nathan Katz, Chesut Hill, Massachusetts, Brook Hill, 1977.

19. Charles, R. J., "Dynamic Fatigue of Glass," Journal of Applied Physics, December, 1958.

20. Pletka, B. J., and Wiederhorn, S. M., "A Comparison of Failure Predictions by Strength and Fracture Mechanics Techniques," Journal of Materials Science, 17 (1982).

21. Govila, R. K., "Material Parameters for Life Prediction ... Ceramics," Ceramics for High Performance Applications-III, e Edward M. Lenoe, R. Nathan Katz, and John J. Burke, New York: Plenum Press, 1983.

22. Bury, K. V., Statistical Models in Applied Science, New York: John Wiley, 1975.

23. Paluszny, A., and Wu, W., "Probabilistic Aspects of Designing with Ceramics," ASME paper 77-GT-41, 1977.

24. Quinn, G. D., and Quinn, J. B., "Slow Crack Growth in Hot-Pressed Silicon Nitride," Fracture Mechanics of Ceramics 6, New York: Plenum Press, to be published.

25. Swank, L. R., "Ceramic Life Prediction Methodology-Analytical Assessment of Selected Time Dependent Test Results," Tech. Rept. AMMRC to be published.

26. Govila, R. K., Methodology for Ceramic Life Prediction and Related Proof Testing, U. S. Department of Energy, 1978.

27. Annis, C. G. and Cargill, J. S., "Modified Double Torsion Method for Measuring Crack Velocity in NC-132," Fracture Mechanics of Ceramics, Volume 4. Ed. R. C. Brandt, D. P. H. Hasselman, and F. F. Lange, New York: Plenum Press, 1977.

28. Larsen, D. C., Property Screening and Evaluation of Ceramic Turbine Engine Materials, Chicago, ITT Research Institute, 1979.

29. Smith, F. W., Emery, A. F., and Kobayashi, A. S. "Stress Intensity Factors for Penny Shaped Cracks," Journal of Applied Mechanics, December, 1967.

30. Tighe, N. J., "The Structure of Slow Crack Interfaces in Silicon Nitride," Journal of Material Science, 13 (1978).

31. Evans, A. G., "High Temperature Slow Crack Growth in Ceramic Materials," Ceramics for High Performance Applications, Ed. John J. Burke, Alvin E. Gorum, and R. Nathan Katz, Chesnut Hill, Massachusetts, Brook Hill, 1974.

32. Chen, E. P. and Hasselman, D. P. H., "Comparison of the High Temperature Thermal Fatigue Resistance of Hot-Pressed Silicon Nitride and Silicon Carbide," Journal of the American Ceramic Society, November-December, 1976.

APPENDIX A

Stress-Rupture Formula

Use of the power relation of crack velocity as a function of stress intensity[4,5],

$$V = AK_I^n \qquad \text{A-1}$$

leads to a reliability versus time equation of the form[12,14]

$$R = R_{ff}^{\left(1+\frac{\sigma^2 t}{B}\right)^{\frac{m}{n-2}}} . \qquad \text{A-2}$$

Examination of the experimental evidence from a number of stress rupture tests indicate that the results fit an equation of the form

$$R = R_{ff} \exp\left(-\phi(t)\right) \qquad \text{A-3}$$

where $\phi(t)$ is some empirical relationship of the variables that describe the time dependent behavior of the material. For a constant temperature these variables are the stress, the volume, and the time. The form of $\phi(t)$ is assumed to be

$$\phi(t) = C \left(\frac{\sigma_2}{\sigma_1}\right)^n \left(\frac{Veff_2}{Veff_1}\right)^y \frac{t_2}{t_1} . \qquad \text{A-4}$$

The subscript 1 applies to the database from which the constants C, n, y, σ_1, and t_1 are determined. Subscript 2 applies to the element for which reliability is being calculated.

The crack velocity exponent was chosen because stress rupture tests in magnesia doped silicon nitrides are described by[10]

$$\sigma^n t = \text{constant} \qquad \text{A-5}$$

when plotted as stress versus time. The effective volume was used as taken from Weibull theory to correct for size differences between the elements. Equation A-4 may be modified to use the characteristic strength of the structure by substituting the following equation given by Paluszny and Wu[23].

$$V_{eff} = \left(\frac{\sigma_o}{\sigma_\theta}\right)^m \qquad \text{A-6}$$

Since at the same temperature $\sigma_{o1} = \sigma_{o2}$ equation A-4 becomes

$$\phi(t) = C\left(\frac{\sigma_2}{\sigma_1}\right)^n \left(\frac{\sigma_{\theta_1}}{\sigma_{\theta_2}}\right)^{y\,m} \frac{t_2}{t_1} \qquad \text{A-7}$$

For a MOR bar σ_θ is the characteristic modulus of rupture, MOR, which makes the application of Equation A-7 relatively simple. Substitution of Equation A-7 into Equation A-3 yields the form of the stress rupture equation used.

$$R = R_{ff} \exp\left(-C\left(\frac{\sigma_2}{\sigma_1}\right)^n \left(\frac{\sigma_{\theta_1}}{\sigma_{\theta_2}}\right)^{y\,m} \frac{t_2}{t_1}\right) \qquad \text{A-8}$$

Equation A-8 is for one temperature. Data was available at three temperatures 1100°C, 1200°C, and 1300°C. For intermediate temperatures $\sigma_{\theta 1}$ n, and m were linearly interpolated.

To apply this equation to the disc, the characteristic strength, $\sigma_{\theta 2}$, of each element was calculated, as well as the fast fracture reliability, R_{ff}. The reliability for the entire disc was calculated from

$$R = R_1 \cdot R_2 R_3 \ldots R_q. \qquad \text{A-9}$$

The form of Equation A-8 makes it less sensitive to the calculation of fast fracture reliability than Equation A-2. In equation A-2 the fast fracture reliability is raised to a power; therefore, the result is very sensitive to the fast fracture reliability. Equation A-4 has a volume correction in its time dependent term which appears to be necessary since ceramics are proven to be sensitive to volume in fast fracture and this should be true in static fatigue. Temperature dependence can be included in equation A-4 by the use of another term so that $\phi(t)$ become

$$\phi(t) = C\left(\frac{\sigma_2}{\sigma_1}\right)^n \left(\frac{V_{eff_2}}{V_{eff_1}}\right)^y \left(\frac{T_2}{T_1}\right)^z \frac{t_1}{t_2}\,. \qquad \text{A-10}$$

This was not done in this study because of the lack of sufficient data to determine z. In this study the temperature dependence was handled by considering n, V_{eff} , and y as functions of temperature.

To utilize the empirical stress rupture formula given here requires a body of stress rupture data from which the empirical constants can be determined. The data base was taken from Quinn[24] and Trantina[9] and the results are given in Table VII. The reference stress was taken directly from Quinn's curves of stress versus time using time equals one hour, the reference time. The stress given by Quinn was multiplied by .82 to account for creep[25]. The crack velocity exponents were taken from Quinn's graph. The reference characteristic MOR is the expected MOR scaled to the size bar used by Quinn. The MOR exponent was determined by the amount required to correct for the difference in bar size and loading configuration between Quinn's and Trantina's tests. They used different effective volumes.

The formula does not necessarily give good predictions in all cases as illustrated in Fig. A-1. This shows a prediction for stress rupture data of Govila[26] taken on a different size bar than Quinn or Trantina used. The result is poor. One possible explanation may be billet to billet variation of the material. The applicability of the proposed empirical formula requires further investigation; however, it was proposed in this report as the method that gave the best result.

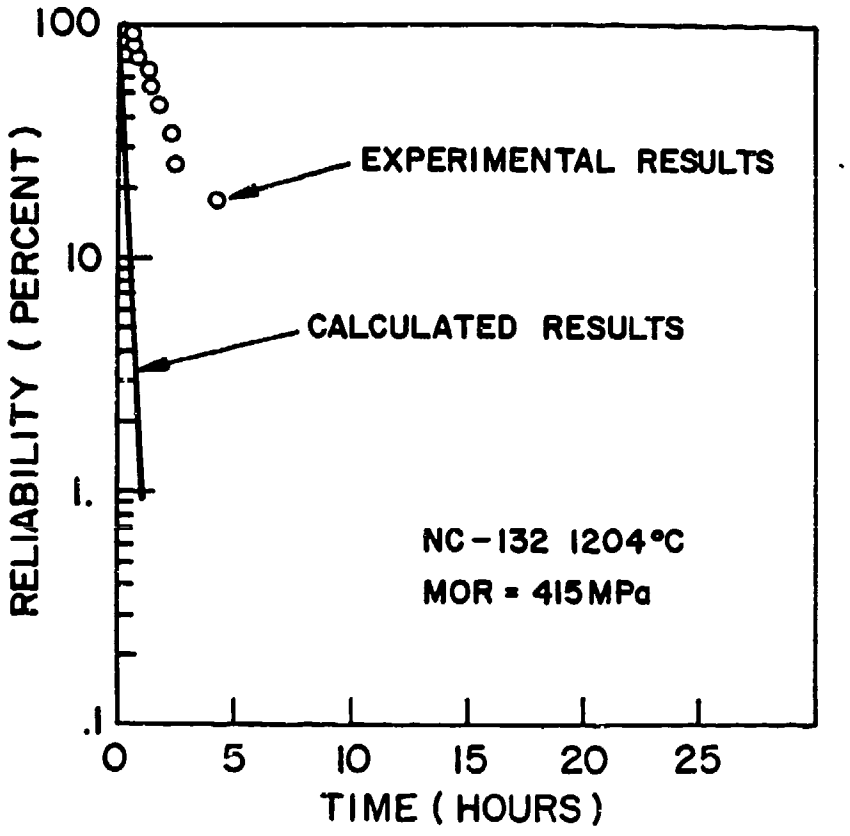

Figure A-1 - Experimental and Calculated Reliability Comparison For 415 MPa Stress Rupture Tests.

APPENDIX B

Calculation of Constant "B"

The calculation of time dependent reliabilities is based on the power relation of crack velocity as a function of stress intensity factor.

$$V = AK_I^n \qquad B\text{-}1$$

The values of A and n are determined experimentally, so a literature search was conducted to find published values to utilize for design and analysis. Table III gives the experimental values that were found. The experimental values were published in graphical or numerical form and the manner of presentation is shown on the table. In the cases of graphical publication the numerical values were found by taking values of velocity, "V", and stress intensity factor, "K_I", from the graph and substituting into Eqn. B-1. It should be noted that considerable error in the determination of A and n may result from this procedure. Cargill and Annis published their results graphically; however, they furnished the values of A and n determined by least squares fitting of their data. The A and n values of Annis and Cargill[27] and Govila[21] were used in this program.

The values of A and n available are published for 930°C, 1200°C, and 1300°C. Reliability calculation requires values for A and n at the centroidal temperature of each finite element of the finite element grid shown in Fig. 2. To obtain the required values, linear interpolation was used.

The critical stress intensity factor for the material is an important parameter when double torsion data is used to calculate time dependent reliability. Larsen[28] presented graphical data for hot pressed silicon nitride and the numerical values used are shown in Table IV. Also required for the use of double torsion data is an assumption about the shape of the flaw, so that the stress intensity factor coefficient may be determined. For this program the flaws were assumed to be penny shaped internal flaw with a stress intensity factor coefficient[29] of $2/\sqrt{\pi}$.

As shown in Fig. 15 the value of "B" must be computed before reliability versus time can be calculated and the following equations show the evaluation of "B" at 1200°C with the required material and geometric constants and their sources.

		References
n	$= 27.4$	27
A	$= 1.58 \times 10^{-23} \frac{m}{sec} \frac{1}{(MPa\sqrt{m})^n}$	27
K_{IC}	$= 7.2$ MPa$\sqrt{m}$	28
Y	$= 2/\sqrt{\pi}$	29

$$B = \frac{2}{(n-2)Y^2 A K_{IC}^{n-2}}$$

$$B = \frac{2}{(27.4-2)(\frac{2}{\sqrt{\pi}})^2\ 1.58 \times 10^{-23} \times (7.2)^{27.4-2}} \times \frac{hr.}{3600\ sec}$$

$$B = 0.000182\ MPa^2 - hr.$$

An alternate data base to use for predicting time dependent failure is stress rate data. The NC-132 stress rate data is given in Table V[26]. Reference 26 gives data for several stress rates, but the lowest available stress rate and corresponding fracture strength was chosen on the assumption that slow stress rate result was most applicable for predicting stress rupture results. As shown on Fig. 16 the value of "B" must be evaluated before reliability versus time can be calculated and the following equations show a typical calculation.

Temperature = 1204°C

			Reference
n	=	19.9	26
σ_f	=	485 MPa	26
$\dot{\sigma}$	=	0.8 MPa/min.	26

$$B = \frac{\sigma_f^3}{\dot{\sigma}(n+1)}$$

$$B = \frac{(485)^3}{0.8x(19.9+1)} \times \frac{hr.}{60\ min.}$$

$$B = 113720\ MPa^2 - hr.$$

APPENDIX C NOMENCLATURE

A	Premultiplier in crack velocity equation, meter/second (MPa-meter)^n.
B	Constant in reliability versus time equation, MPa^2-hr.
C	Constant in stress rupture equation.
i	Order of a specimen.
k	Index on Operator II.
K_{Ic}	Critical stress intensity, a material parameter, MPa/meter.
K_I	Stress intensity Mpa$\sqrt{}$meter.
m	Weibull modulus.
MOR_o	Characteristic modulus of rupture, MPa.
n	Crack velocity exponent.
N	Initial sample size.
$\phi(t)$	Function in stress rupture equation.
q	Number of elements in the structure.
R	Reliability as a function of time.
R_{ff}	Fast fracture reliability.
$\hat{R}(X')$	Maximum likelihood estimator of reliability.
σ	Stress, MPa.
σ_θ	Characteristic strength of the structure, MPa.
σ_f	Fracture stress, MPa.
$\dot{\sigma}$	Stress rate, MPa/min.
σ_o	Weibull parameter, MPa/(meter^3) 1/m.
T	Temperature, °C.
t	Time, hours.
v	Volume, meter^3.
V	Crack velocity, meter/sec.
V_{eff}	Effective volume, meter^3
Y	Stress intensity factor coefficient, non-dimensional.
y	Exponent on effective volume.
z	Exponent on temperature.

APPENDIX D

Data on Norton Billets

As part of the billet certification the Norton Company supplied strength data on each billet. The data was taken on test bars of .125x.128x1.375 inches in 4 point bending with the upper span of 0.5 inch and the lower span of 1.0 inch. Eight bars were tested from each billet. The characterisitic MOR and Weibull modulus were calculated using maximum likelihood estimator techniques[18] and the result was scaled to .25 in. width by .125 in. height size bar with an upper span of .375 in. and a lower span of .75 in. using the following formula[17].

$$\frac{MOR_B}{MOR_A} = \left(\frac{b_A h_A}{b_B h_B}\right)^{\frac{1}{m}} \left(\frac{L_{A_1} + m L_{A_2}}{L_{B_1} + m L_{B_2}}\right)^{\frac{1}{m}} \qquad \text{D-1}$$

Billet Record	Characteristic MOR psi	Weibull Modulus	Density gm/cm^3	History of Disc
1313	135000	8.78	3.25	Failed on start up
1314	133000	17.4	3.23	13.80 hours
1318	142000	17.4	3.23	8.50 hours
1319	133000	7.57	3.24	Censored at 24 hours
1321	132000	9.40	3.26	Censored at 13 hours
1322	136000	10.2	3.26	7.17 hours
1323	128000	12.7	3.25	Censored at 25 hours
1324	133000	13.4	3.25	18.58 hours
1333	136000	16.4	3.25	0.20 hours
1335	138000	8.26	3.24	18.27 hours
1336	126000	7.10	3.24	Failed on start up
1337	138000	15.8	3.23	Censored at 24 hours

TABLE I

Thermal Properties

	Temperature °F	Thermal Conductivity $\frac{Btu}{hr\ ft\ °F}$	Specific Heat $Btu/lb_m-°F$
Spin Disc and Ceramic	70.	17	.18
Curvic Spacer Material	500.	15.	.23
Hot Pressed Silicon Nitride	1000.	13.	.26
Density = 3.18 gm/cm^3	1500.	11.	.29
	2000.	9.2	.33
	2500.	8.0	.32
Nut Material	0.	6.0	.10
Inconel X-750	3000.	20.5	.18
Density = 8.30 gm/cm^3			
Tie Bolt Material	0.	6.0	.10
Inconel X-718	3000.	21.8	.10
Density = 8.19 gm/cm^3			
Compression Member	0.	6.5	.11
Material	3000.	25.2	.11
A-286			
Density = 7.91 gm/cm^3			
Shaft Material	0.	21.7	.11
AMS 6265	3000.	21.7	.11
Density = 7.83 gm/cm^3			
Curvic Material	70.	3.99	.18
	500.	3.87	.23
Density = 3.18 gm/cm^3	1000.	3.72	.26
	1500.	3.54	.29
	2000.	3.33	.33
	2500.	3.16	.32

	Temperature °F	Thermal Conductivity $\frac{Btu}{hr\ ft\ °F}$	Specific Heat $\frac{Btu}{lbm°F}$	Density $\frac{lbm}{ft^3}$
Air	0	.013	.239	.0863
	100	.015	.240	.0680
	500	.023	.247	.0392
	800	.028	.256	.0299
	1000	.032	.262	.0258
	1500	.040	.276	.0192
	2000	.047	.286	.0153
	2500	.051	.292	.0127
	3000	.054	.297	.0108

TABLE II

Elastic Properties

NC-132 Hot Pressed Silicon	Temperature	Young's Modulus	Poisson's Ratio	Shear Modulus	Coefficient of Thermal Expansion in/in/°F
Density = 3.18 gm/cm^3	°F	x10^{6}psi		x10^{6}psi	x10^{-6}
	78	41.9	.219	17.1	.74
	500	41.9	.203	17.5	.97
	1000	41.8	.190	17.5	1.32
	1500	40.6	.189	17.1	1.53
	2000	38.7	.194	16.1	1.68
	2500	35.4	.194	14.3	1.82

Reference 13

TABLE III

Crack Velocity Parameters Survey

Material	Temp. °C	A	Crack Velocity Exponent n	Ref.	Form of Data Presentation
HPSN NC-132	930	6.18×10^{-56}	74.7	27	Graphical
HPSN NC-132	1200	1.58×10^{-23}	27.4	27	Graphical
HPSN NC-132	1300	4.3×10^{-9}	5.6	21	Numerical
HPSN NC-132	1350	7.9×10^{-9}	5.6	21	Numerical
HPSN NC-132	1400	1×10^{-7}	5.25	21	Numerical
HPSN NC-132	1200	1.21×10^{-31}	35.4	30	Graphical
HPSN NC-132	1400	9×10^{-8}	5.8	30	Graphical
HPSN HS-130	1250	1.41×10^{-14}	10.5	31	Graphical
HPSN HS-130	1300	9.31×10^{-14}	11.5	31	Graphical
HPSN HS-130	1350	9.83×10^{-13}	10.2	31	Graphical
HPSN HS-130	1400	3.05×10^{-12}	10.6	31	Graphical
HPSN HS-130	1200	2.56×10^{-59}	73.3	31	Graphical
HPSN HS-130	1400	8.22×10^{-8}	4.93	31	Graphical
HPSN	1000 to 1400	5×10^{-14}	6	32	Numerical

TABLE IV

Critical Stress Intensity Factor

Temperature °C	Stress Intensity Factor MPa√m
18	5.
930	5.
1200	7.2
1300	11.0

Reference 28

TABLE V

Stress Rate Data of Norton NC-132 HPSN

Temperature °C	Characteristic MOR MPa	Weibull Modulus	Stress Rate MPa/min.	Crack Velocity Exponent	Number of Samples
21	787.	6.5	1870.0	72.2	30
704	730.	6.0	1.8	72.2	5
871	818.	8.5	1.8	72.2	5
1038	666.	9.9	1.5	72.7	5
1204	485.	8.0	.8	19.9	5
1371	313.	11.2	91.0	17.2	15

Reference 26

TABLE VI

Summary of Discs Tested

Discs Number	Order Number i	Failure Time Hours	Censoring Time Hours	$\frac{N-i}{N-i+1}$	Reliability $\hat{R}(X_i)$
NC-1333	1	.20		9/10	.90
NC-1322	2	7.17		8/9	.80
NC-1318	3	8.50		7/8	.70
NC-1321	4		13.00		-
NC-1314	5	13.83		5/6	.58
NC-1335	6	18.27		4/5	.47
NC-1324	7	18.58		3/4	.35
NC-1319	8		24.00		
NC-1337	9		24.00		
NC-1323	10		25.00		

TABLE VII

Stress Rupture Data Base

Temp. °C	Constant	Reference Stress MPa	Crack Vel. Exp.	Reference Char. Mpa	MOR Exp.	Reference Time Hours
1100	.69	402	19	634.8	8.15	1.
1200	.69	295	12	517.0	4.80	1.
1300	.69	230	10	411.1	4.50	1.

Reference 24

DISTRIBUTION LIST

No. of Copies	To
	Office of the Under Secretary of Defense for Research and Engineering, The Pentagon, Washington, DC 20301
1	ATTN: Mr. J. Persh
1	Dr. G. Gamota
12	Commander, Defense Technical Information Center, Cameron Station, Building 5, 5010 Duke Street, Alexandria, VA 22314
1	National Technical Information Service, 5285 Fort Royal Road, Springfield, VA 22161
	Director, Defense Advanced Research Projects Agency, 1400 Wilson Boulevard, Arlington, VA 22209
1	ATTN: Dr. A. Bement
1	Dr. Van Reuth
1	MAJ Harry Winsor
	Battelle Columbus Laboratories, Metals and Ceramics Information Center, 505 King Avenue, Columbus, OH 43201
1	ATTN: Mr. Winston Duckworth
1	Dr. D. Niesz
1	Dr. R. Wills
	Deputy Chief of Staff, Research, Development, and Acquisition, Headquarters, Department of the Army, Washington, DC 20301
1	ATTN: DAMA-ARZ
1	DAMA-CSS, Dr. J. Bryant
	Commander, U.S. Army Medical Research and Development Command, Fort Detrick, Frederick, MD 21701
1	ATTN: SGRD-SI, Mr. Lawrence L. Ware, Jr.
	Commander, Army Research Office, P.O. Box 12211, Research Triangle Park, NC 27709
1	ATTN: Information Processing Office
1	Dr. G. Mayer
1	Dr. J. Hurt
	Commander, U.S. Army Materiel Development and Readiness Command, 5001 Eisenhower Avenue, Alexandria, VA 22333
1	ATTN: DRCDMD-ST
1	DRCLDC
	Commander, Harry Diamond Laboratories, 2800 Powder Mill Road, Adelphi, MD 20783
1	ATTN: Mr. A. Benderly
1	Technical Information Office
1	DELHD-RAE
	Commander, U.S. Army Missile Command, Redstone Arsenal, AL 35809
1	ATTN: Mr. P. Ormsby
1	Technical Library
	Commander, U.S. Army Aviation Research and Development Command, 4300 Goodfellow Boulevard, St. Louis, MO 63120
1	ATTN: DRDAV-EGX
1	DRDAV-QE
	Commander, U.S. Army Tank-Automotive Command, Warren, MI 48090
1	ATTN: Dr. W. Bryzik
1	Mr. E. Hamperian
1	D. Rose
1	DRSTA-RKA
1	DRSTA-UL, Technical Library
1	DRSTA-R
	Commander, U.S. Army Armament Research and Development Command, Dover, NJ 07801
1	ATTN: Dr. G. Vezzoli
1	Technical Library
	Commander, U.S. Army Armament Materiel Readiness Command, Rock Island, IL 61299
1	ATTN: Technical Library
	Commander, Aberdeen Proving Ground, MD 21005
1	ATTN: DRDAR-CLB-PS, Mr. J. Vervier
	Commander, U.S. Army Mobility Equipment Research and Development Command, Fort Belvoir, VA 22060
1	ATTN: DRDME-EM, Mr. W. McGovern
1	DRDME-V, Mr. E. York
	Director, U.S. Army Ballistic Research Laboratory, Aberdeen Proving Ground, MD 21005
1	ATTN: DRDAR-TSB-S (STINFO)
	Commander, U.S. Army Test and Evaluation Command, Aberdeen Proving Ground, MD 21005
1	ATTN: DRSTE-ME
	Commander, U.S. Army Foreign Science and Technology Center, 220 7th Street, N.E., Charlottesville, VA 22901
1	ATTN: Military Tech, Mr. W. Marley
	Commander, Watervliet Arsenal, Watervliet, NY 12189
1	ATTN: Dr. T. Davidson
	Director, Eustis Directorate, U.S. Army Mobility Research and Development Laboratory, Fort Eustis, VA 23604
1	ATTN: Mr. J. Robinson, DAVDL-E-MOS (AVRADCOM)
1	Mr. C. Walker
	Chief of Naval Research, Arlington, VA 22217
1	ATTN: Code 471
1	Dr. A. Diness
1	Dr. R. Pohanka
	Naval Research Laboratory, Washington, DC 20375
1	ATTN: Dr. J. M. Krafft - Code 5830
1	Mr. R. Rice
	Headquarters, Naval Air Systems Command, Washington, DC 20360
1	ATTN: Code 5203
1	Code MAT-042M
1	Mr. I. Macklin
	Commander, Naval Weapons Center, China Lake, CA 93555
1	ATTN: Mr. F. Markarian
	Commander, U.S. Air Force of Scientific Research, Building 410, Bolling Air Force Base, Washington, DC 20332
1	ATTN: MAJ W. Simmons
	Commander, U.S. Air Force Wright Aeronautical Laboratories, Wright-Patterson Air Force Base, OH 45433
1	ATTN: AFWAL/MLLM, Dr. N. Tallan
1	AFWAL/MLLM, Dr. H. Graham
1	AFWAL/MLLM, Dr. R. Ruh
1	AFWAL/MLLM, Dr. A. Katz
1	AFWAL/MLLM, Mr. K. S. Mazdiyasni
1	Aero Propulsion Labs, Mr. R. Marsh
	National Aeronautics and Space Administration, Washington, DC 20546
1	ATTN: Mr. G. C. Deutsch - Code RW
1	Mr. J. Gangler
1	AFSS-AD, Office of Scientific and Technical Information
	National Aeronautics and Space Administration, Lewis Research Center, 21000 Brookpark Road, Cleveland, OH 44135
1	ATTN: J. Accurio, USAMRDL
1	Dr. H. B. Probst, MS 49-1
1	Dr. W. Brown, Jr., MS 49-6
1	Dr. S. Dutta
1	Mr. S. Grisaffe
	National Aeronautics and Space Administration, Langley Research Center, Center, Hampton, VA 23665
1	ATTN: Mr. J. Buckley, Mail Stop 387
	Department of Energy, Division of Transportation, 20 Massachusetts Avenue, N.W., Washington, DC 20545
1	ATTN: Mr. George Thur (TEC)
1	Mr. Robert Schulz (TEC)
1	Mr. John Neal (CLNRT)
1	Mr. Steve Wander (Fossil Fuels)
	Department of Transportation, 400 Seventh Street, S.W., Washington, DC 20590
1	ATTN: Mr. M. Lauriente
	National Bureau of Standards, Washington, DC 20234
1	ATTN: Dr. S. Wiederhorn
	National Research Council, National Materials Advisory Board, 2101 Constitution Avenue, Washington, DC 20418
1	ATTN: D. Groves
1	R. M. Spriggs
	National Science Foundation, Washington, DC 20550
1	ATTN: B. A. Wilcox

No. of Copies	To
	Admiralty Materials Technology Establishment, Poole, Dorset BH16 6JU, UK
1	ATTN: Dr. D. Godfrey
1	Dr. M. Lindley
	AiResearch Manufacturing Company, AiResearch Casting Company, 2525 West 190th Street, Torrance, CA 90505
1	ATTN: Mr. K. Styhr
	AiResearch Manufacturing Company, Materials Engineering Dept., 111 South 34th Street, P.O. Box 5217, Phoenix, AZ 85010
1	ATTN: Mr. D. W. Richerson, MS 93-393/503-44
	AVCO Corporation, Applied Technology Division, Lowell Industrial Park, Lowell, MA 01887
1	ATTN: Dr. T. Vasilos
	Carborundum Company, Research and Development Division, P.O. Box 1054, Niagara Falls, NY 14302
1	ATTN: Dr. J. A. Coppola
	Case Western Reserve University, Department of Metallurgy, Cleveland, OH 44106
1	ATTN: Prof. A. H. Heuer
	Cummins Engine Company, Columbus, IN 47201
1	ATTN: Mr. R. Kamo
	Deposits and Composites, Inc., 1821 Michael Faraday Drive, Reston, VA 22090
1	ATTN: Mr. R. E. Engdahl
	Electric Power Research Institute, P.O. Box 10412, 3412 Hillview Avenue, Palo Alto, CA 94304
1	ATTN: Dr. A. Cohn
	European Research Office, 223 Old Maryleborne Road, London, NW1 - 5the, England
1	ATTN: Dr. R. Quattrone
1	LT COL James Kennedy
	Ford Motor Company, Turbine Research Department, 20000 Rotunda Drive, Dearborn, MI 48121
1	ATTN: Mr. A. F. McLean
1	Mr. E. A. Fisher
1	Mr. J. A. Mangels
1	Mr. R. Govila
	General Electric Company, Research and Development Center, Box 8, Schenectady, NY 12345
1	ATTN: Dr. R. J. Charles
1	Dr. C. D. Greskovich
1	Dr. S. Prochazka
	General Motors Corporation, AC Spark Plug Division, Flint, MI 48556
1	ATTN: Dr. M. Berg
	Georgia Institute of Technology, EES, Atlanta, GA 30332
1	ATTN: Mr. J. D. Walton
	GTE Laboratories, Waltham Research Center, 40 Sylvan Road, Waltham, MA 02154
1	ATTN: Dr. C. Quackenbush
1	Dr. W. H. Rhodes
	IIT Research Institute, 10 West 35th Street, Chicago, IL 60616
1	ATTN: Mr. S. Bortz, Director, Ceramics Research
	Institut fur Werkstoff-Forschung, DFVLR, 505 Porz-Wahn, Linder Hohe, Germany
1	ATTN: Dr. W. Bunk
	International Harvester, Solar Division, 2200 Pacific Highway, P.O. Box 80966, San Diego, CA 92138
1	ATTN: Dr. A. Metcalfe
1	Ms. M. E. Gulden

No. of Copies	To
	Kawecki Berylco Industries, Inc., P.O. Box 1462, Reading, PA 19603
1	ATTN: Mr. R. J. Longenecker
	Martin Marietta Laboratories, 1450 South Rolling Road, Baltimore, MD 21227
1	ATTN: Dr. J. Venables
	Massachusetts Institute of Technology, Department of Metallurgy and Materials Science, Cambridge, MA 02139
1	ATTN: Prof. R. L. Coble
1	Prof. H. K. Bowen
1	Prof. W. D. Kingery
	Midwest Research Institute, 425 Volker Boulevard, Kansas City, MO 64110
1	ATTN: Mr. Gordon W. Gross, Head, Physics Station
	Norton Company, Worcester, MA 01606
1	ATTN: Dr. N. Ault
1	Dr. M. L. Torti
	Pennsylvania State University, Materials Research Laboratory, Materials Science Department, University Park, PA 16802
1	ATTN: Prof. R. E. Tressler
1	Prof. R. Bradt
1	Prof. V. S. Stubican
	RIAS, Division of the Martin Company, Baltimore, MD 21203
1	ATTN: Dr. A. R. C. Westwood
	Stanford Research International, 333 Ravenswood Avenue, Menlo Park, CA 94025
1	ATTN: Dr. P. Jorgensen
1	Dr. D. Rowcliffe
	State University of New York at Stony Brook, Department of Materials Science, Long Island, NY 11790
1	ATTN: Prof. Franklin F. Y. Wang
	United Technologies Research Center, East Hartford, CT 06108
1	ATTN: Dr. J. Brennan
1	Dr. F. Galasso
	University of California, Lawrence Livermore Laboratory, P.O. Box 808, Livermore, CA 94550
1	ATTN: Dr. C. F. Cline
	University of Florida, Department of Materials Science and Engineering, Gainesville, FL 32601
1	ATTN: Dr. L. Hench
	University of Newcastle Upon Tyne, Department of Metallurgy and Engineering Materials, Newcastle Upon Tyne, NE1 7 RU, England
1	ATTN: Prof. K. H. Jack
	University of Washington, Ceramic Engineering Division, FB-10, Seattle, WA 98195
1	ATTN: Prof. James I. Mueller
	Westinghouse Electric Corporation, Research Laboratories, Pittsburgh, PA 15235
1	ATTN: Dr. R. J. Bratton
	Director, Army Materials and Mechanics Research Center, Watertown, MA 02172
2	ATTN: DRXMR-PL
1	DRXMR-PR
1	DRXMR-K
10	DRXMR-MC, Dr. R. Katz
10	DRXMR-SM, Dr. E. Lenoe

Army Materials and Mechanics Research Center,
Watertown, Massachusetts 02173
CERAMIC LIFE PREDICTION METHODOLOGY -
HOT SPIN DISC LIFE PROGRAM
R. R. Baker, L. R. Swank, and J. C. Caverly

AD ____________
UNCLASSIFIED
UNLIMITED DISTRIBUTION

Technical Report AMMRC TR 83-44, August 1983, 39 pp - illus-tables, Contract DAAG46-77-C-0028, Interim Report

Key Words

Brittle design
Ceramics
High temperature
Materials
Silicon nitride
Silicon carbide
Mechanical properties

A rotating disc was designed to fail due to time-dependent mechanisms. Several discs were fabricated and an existing test rig was developed to test the discs at design conditions. Ten discs were tested at steady state under the design conditions of 2300°F rim temperature and 50,000 rpm for periods of 0.20 hours to 25 hours. An experimental failure distribution was obtained for the ten discs and presented as reliability versus time. Three different data bases were used to calculate reliability versus time and the results were compared to the experimental results.

Army Materials and Mechanics Research Center,
Watertown, Massachusetts 02173
CERAMIC LIFE PREDICTION METHODOLOGY -
HOT SPIN DISC LIFE PROGRAM
R. R. Baker, L. R. Swank, and J. C. Caverly

AD ____________
UNCLASSIFIED
UNLIMITED DISTRIBUTION

Technical Report AMMRC TR 83-44, August 1983, 39 pp - illus-tables, Contract DAAG46-77-C-0028, Interim Report

Key Words

Brittle design
Ceramics
High temperature
Materials
Silicon nitride
Silicon carbide
Mechanical properties

A rotating disc was designed to fail due to time-dependent mechanisms. Several discs were fabricated and an existing test rig was developed to test the discs at design conditions. Ten discs were tested at steady state under the design conditions of 2300°F rim temperature and 50,000 rpm for periods of 0.20 hours to 25 hours. An experimental failure distribution was obtained for the ten discs and presented as reliability versus time. Three different data bases were used to calculate reliability versus time and the results were compared to the experimental results.

Army Materials and Mechanics Research Center,
Watertown, Massachusetts 02173
CERAMIC LIFE PREDICTION METHODOLOGY -
HOT SPIN DISC LIFE PROGRAM
R. R. Baker, L. R. Swank, and J. C. Caverly

AD ____________
UNCLASSIFIED
UNLIMITED DISTRIBUTION

Technical Report AMMRC TR 83-44, August 1983, 39 pp - illus-tables, Contract DAAG46-77-C-0028, Interim Report

Key Words

Brittle design
Ceramics
High temperature
Materials
Silicon nitride
Silicon carbide
Mechanical properties

A rotating disc was designed to fail due to time-dependent mechanisms. Several discs were fabricated and an existing test rig was developed to test the discs at design conditions. Ten discs were tested at steady state under the design conditions of 2300°F rim temperature and 50,000 rpm for periods of 0.20 hours to 25 hours. An experimental failure distribution was obtained for the ten discs and presented as reliability versus time. Three different data bases were used to calculate reliability versus time and the results were compared to the experimental results.

Army Materials and Mechanics Research Center,
Watertown, Massachusetts 02173
CERAMIC LIFE PREDICTION METHODOLOGY -
HOT SPIN DISC LIFE PROGRAM
R. R. Baker, L. R. Swank, and J. C. Caverly

AD ____________
UNCLASSIFIED
UNLIMITED DISTRIBUTION

Technical Report AMMRC TR 83-44, August 1983, 39 pp - illus-tables, Contract DAAG46-77-C-0028, Interim Report

Key Words

Brittle design
Ceramics
High temperature
Materials
Silicon nitride
Silicon carbide
Mechanical properties

A rotating disc was designed to fail due to time-dependent mechanisms. Several discs were fabricated and an existing test rig was developed to test the discs at design conditions. Ten discs were tested at steady state under the design conditions of 2300°F rim temperature and 50,000 rpm for periods of 0.20 hours to 25 hours. An experimental failure distribution was obtained for the ten discs and presented as reliability versus time. Three different data bases were used to calculate reliability versus time and the results were compared to the experimental results.